Measurement of the Cosmic-Ray Antiproton Spectrum at Solar Minimum with a Long-Duration Balloon Flight over Antarctica

K. Abe,[1] H. Fuke,[2] S. Haino,[3] T. Hams,[4] M. Hasegawa,[3] A. Horikoshi,[3] K. C. Kim,[5] A. Kusumoto,[1] M. H. Lee,[5]
Y. Makida,[3] S. Matsuda,[3] Y. Matsukawa,[1] J. W. Mitchell,[4] J. Nishimura,[6] M. Nozaki,[3] R. Orito,[1] J. F. Ormes,[7] K. Sakai,[6,*]
M. Sasaki,[4] E. S. Seo,[5] R. Shinoda,[6] R. E. Streitmatter,[4] J. Suzuki,[3] K. Tanaka,[3] N. Thakur,[7] T. Yamagami,[2]
A. Yamamoto,[3,6] T. Yoshida,[2] and K. Yoshimura[3]

[1]*Kobe University, Kobe, Hyogo 657-8501, Japan*
[2]*Institute of Space and Astronautical Science, Japan Aerospace Exploration Agency (ISAS/JAXA),
Sagamihara, Kanagawa 229-8510, Japan*
[3]*High Energy Accelerator Research Organization (KEK), Tsukuba, Ibaraki 305-0801, Japan*
[4]*NASA-Goddard Space Flight Center (NASA-GSFC), Greenbelt, Maryland 20771, USA*
[5]*IPST, University of Maryland, College Park, Maryland 20742, USA*
[6]*The University of Tokyo, Bunkyo, Tokyo 113-0033, Japan*
[7]*University of Denver, Denver, Colorado 80208, USA*
(Received 28 July 2011; revised manuscript received 21 October 2011; published 31 January 2012)

The energy spectrum of cosmic-ray antiprotons ($\bar{p}$'s) from 0.17 to 3.5 GeV has been measured using 7886 $\bar{p}$'s detected by BESS-Polar II during a long-duration flight over Antarctica near solar minimum in December 2007 and January 2008. This shows good consistency with secondary $\bar{p}$ calculations. Cosmologically primary $\bar{p}$'s have been investigated by comparing measured and calculated $\bar{p}$ spectra. BESS-Polar II data show no evidence of primary $\bar{p}$'s from the evaporation of primordial black holes.

Precise measurement of the cosmic-ray antiproton ($\bar{p}$) spectrum is crucial to investigations of conditions in the early Universe and cosmic-ray propagation. Most cosmic-ray $\bar{p}$'s are produced by interactions of cosmic-ray nuclei with the interstellar gas. The energy spectrum of these "secondary" $\bar{p}$'s peaks near 2 GeV, decreasing sharply below and above due to the kinematics of $\bar{p}$ production and to the local interstellar (LIS) proton spectrum. The secondary $\bar{p}$'s offer a unique probe [1–3] of cosmic-ray propagation and solar modulation. Cosmologically "primary" sources have also been suggested, including the annihilation of dark-matter particles and the evaporation of primordial black holes (PBH) by Hawking radiation [4].

Small PBHs, formed in the early Universe by initial density fluctuations, phase transitions, or the collapse of cosmic strings, might have a significant evaporation rate at the current age of the Universe and could contribute to the measured $\bar{p}$ spectrum at low energies [5]. Because the predicted LIS PBH $\bar{p}$ spectrum peaks at ~ 150 MeV, this would be strongly influenced by solar modulation, so a search is most sensitive at solar minimum [6].

BESS95 + 97 showed that the $\bar{p}$ spectrum peaks around 2 GeV [7], and measurements by BESS and other experiments have shown that $\bar{p}$'s are predominantly secondary [8]. However, the low-energy $\bar{p}$ spectrum measured by BESS95 + 97 at the previous solar minimum was slightly flatter than predicted by secondary models. Although this suggested the possible presence of primary $\bar{p}$'s, the large statistical error of the BESS95 + 97 data did not allow a firm conclusion. BESS-Polar [8–13] was developed to

evaluate the possibility of excess low-energy $\bar{p}$ flux, with unprecedented precision, using long-duration solar-minimum flights over Antarctica. BESS-Polar I flew in December 2004 [14–17], and BESS-Polar II [15] flew near solar minimum in December 2007 and January 2008. Here, we report measurements of cosmic-ray $\bar{p}$'s from 0.17 to 3.5 GeV by BESS-Polar II and discuss the implications for secondary models and possible primary sources.

BESS-Polar is a high-resolution magnetic-rigidity spectrometer. A uniform field of 0.8 T is produced in a thin superconducting solenoid filled with drift-chamber tracking detectors. Particle trajectories are determined by fitting up to 52 hit points with a resolution of ~ 140 μm in the bending plane, giving a magnetic-rigidity ($\equiv Pc/Ze$) resolution of 0.4% at 1 GV and an overall maximum detectable rigidity of 240 GV. Upper (UTOF) and lower (LTOF) scintillator hodoscopes measure time of flight (TOF) and dE/dx and provide the event trigger. For BESS-Polar II $\bar{p}$ measurements, the acceptance is 0.23 m^2 sr. TOF resolution between the UTOF and LTOF is 120 ps, giving a β^{-1} resolution of 2.5%. A threshold-type Cherenkov counter (ACC), using a silica aerogel radiator with optical index $n = 1.03$, rejects e^- and μ^- backgrounds by a factor of 6100 to identify $\bar{p}$'s up to 3.5 GeV [18]. A thin scintillator middle TOF (MTOF) on the lower surface of the solenoid bore detects low-energy particles that cannot penetrate the magnet wall. TOF resolution between the UTOF and MTOF is 320 ps. In the present analysis, the MTOF was used to independently verify the procedure for eliminating

interacting upward-going protons that could mimic low-energy $\bar{p}$'s.

BESS-Polar II was launched on December 23, 2007, from Williams Field, near the U.S. McMurdo Station in Antarctica, observing for 24.5 days with the magnet energized. The float altitude was 34 to 38 km (residual air of 5.8 g/cm^2 on average), and the cutoff rigidity was below 0.5 GV. 4.7×10^9 events were acquired with no in-flight event selection as 13.6 terabytes of data.

In flight, most detectors and instrument systems operated well, with expected performance. Although the central tracker exhibited high-voltage fluctuations, normal resolution was preserved for more than 90% of the observation time by using algorithms that calibrate the tracker over short time intervals and depend on its high-voltage state. Two TOF photomultipliers with high-voltage control problems were turned off, one on a UTOF paddle (of 10) and one on an LTOF paddle (of 12). Requiring two good photomultipliers on each paddle reduced acceptance by ~20%.

Analysis was performed as described in Ref. [17]. The same selection criteria were applied for $\bar{p}$'s and protons because they behave similarly in the symmetric configuration of BESS-Polar, except for deflection direction.

Figure 1 shows β^{-1} versus rigidity plots for events surviving dE/dx and ACC cuts. A clean, narrow band of 7886 $\bar{p}$'s mirrors the protons. The calculated e^- and μ^- background is 0.0%, 1.0%, and 2.3% in the 0.2–1.0, 1.0–2.0, and 2.0–3.5 GeV energy bands. Other
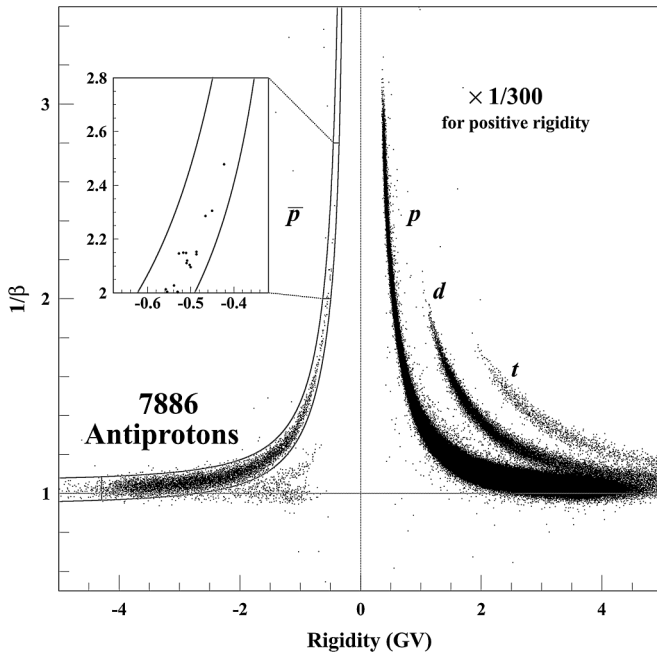

FIG. 1. The β^{-1} versus rigidity plot and $\bar{p}$ mass selection band after dE/dx and ACC cuts. For clarity, only 1 in 300 positive-rigidity events is shown, so only a few e^+ or μ^+ can be seen. The lowest-energy $\bar{p}$'s are shown in the inset figure.

backgrounds, such as albedo, mismeasured positive-rigidity particles, and reentrant albedo, were negligible.

The differential flux of $\bar{p}$'s at the top of atmosphere (Φ_{TOA}) integrated over dE can be expressed as

$$\Phi_{\text{TOA}} dE = (N_{\text{TOI}} - N_{\text{atmos}})/\varepsilon_{\text{air}}/(S\Omega T_{\text{live}}), \quad (1)$$

$$N_{\text{TOI}} = (N_{\bar{p}} - N_{\text{BG}})/(\varepsilon_{\text{det}}\varepsilon_{\text{nonint}}), \quad (2)$$

where T_{live} is live time, $N_{\bar{p}}$ and N_{BG} are numbers of observed $\bar{p}$ candidates and expected background particles, and N_{TOI} is the number of $\bar{p}$'s at the top of instrument. For the present analysis, $T_{\text{live}} = 1\,286\,460$ seconds. The effective geometric acceptance, including noninteraction efficiency ($S\Omega\varepsilon_{\text{nonint}}$), was calculated using GEANT3 as 0.133 ± 0.011 m^2 sr at 0.2 GeV and 0.159 ± 0.008 m^2 sr at 2.0 GeV, with errors estimated from differences relative to GEANT4. The detection efficiency for $\bar{p}$'s (ε_{det}) was calculated using a noninteracting proton sample as $81.4 \pm 0.1\%$ at 0.2 GeV and $60.0 \pm 0.2\%$ at 2.0 GeV. To obtain Φ_{TOA}, corrections were applied for $\bar{p}$ survival probability [19] in the residual atmosphere (ε_{air}) and estimated atmospheric $\bar{p}$ production (N_{atmos}). ε_{air} was estimated as $85.6 \pm 2.0\%$ at 0.2 GeV and $89.8 \pm 2.0\%$ at 2.0 GeV. N_{atmos}, $17.6 \pm 3.2\%$ of the detected $\bar{p}$'s at 0.2 GeV and $27.6 \pm 5.0\%$ at 2.0 GeV, was calculated by solving simultaneous transport equations [19] with adjusted interaction length (λ) and tertiary production [20]. The uncertainty in this calculation is 18.1% $\{= [5.0\%^2(\text{airdepth}) + 8.9\%^2(\lambda) + 15.0\%^2(\text{tertiary})]^{1/2}\}$.

Table I gives the flux of $\bar{p}$'s at TOA from 0.17 to 3.5 GeV with the statistical (first) and systematic (second) errors. The dominant systematics are atmospheric subtraction and detection efficiency. A rapid change in efficiency due to the ACC veto increases the systematic uncertainty in the two highest bins.

Figure 2 shows the BESS-Polar II $\bar{p}$ spectrum with BESS95 + 97 and PAMELA [21] measurements and solar-minimum secondary calculations [6,22–26]. Curve 1 uses Mitsui et al. [6,22] data with force-field modulation of 600 MV from the best fit to the BESS-Polar II proton spectrum. Curve 2 was generated by interpolating model calculations supplied by Bieber et al. [23] for negative solar magnetic field polarity ($A < 0$). The tilt angle of $15°(A < 0)$ is the best fit to the BESS-Polar II proton data. Curve 6 is the published $A > 0$ solar-minimum calculation [23] for comparison to the BESS95 + 97 measurements. Curves 3 [24] and 4 [25] are also published solar-minimum calculations. Curve 5 was generated using the GALPROP model [26] with 600 MV force-field modulation. Improved statistical precision of the measured $\bar{p}$ flux results from 14 and 30 times more events below 1 GeV than BESS95 + 97 and PAMELA, respectively. The BESS-Polar II and PAMELA spectra generally agree in shape but differ in absolute flux. The weighted mean difference, with combined uncertainties, is $14 \pm 5\%$,

TABLE I. $\bar{p}$ flux at the top of atmosphere with statistical (first) and systematic (second) errors. $N_{\bar{p}}$ and N_{BG} are the number of observed $\bar{p}$'s and estimated background events. The mean energy for each range was calculated using the measured $\bar{p}$ energies.

Kinetic energy (GeV) Range	Mean	$N_{\bar{p}}$	N_{BG}	$\bar{p}$ flux (m^{-2} sr^{-1} s^{-1} GeV^{-1})	Kinetic energy (GeV) Range	Mean	$N_{\bar{p}}$	N_{BG}	$\bar{p}$ flux (m^{-2} sr^{-1} s^{-1} GeV^{-1})
0.17–0.23	0.20	29	0.0	$3.56^{+0.88+0.42}_{-0.78-0.42} \times 10^{-3}$	0.98–1.07	1.03	238	0.1	$1.75^{+0.15+0.13}_{-0.15-0.13} \times 10^{-2}$
0.23–0.27	0.25	26	0.0	$4.53^{+1.23+0.53}_{-1.10-0.53} \times 10^{-3}$	1.07–1.17	1.12	283	0.2	$1.91^{+0.15+0.15}_{-0.15-0.15} \times 10^{-2}$
0.27–0.32	0.30	38	0.0	$5.09^{+1.13+0.50}_{-1.03-0.50} \times 10^{-3}$	1.17–1.28	1.23	304	0.6	$1.82^{+0.14+0.14}_{-0.14-0.14} \times 10^{-2}$
0.32–0.37	0.35	69	0.0	$7.55^{+1.16+0.43}_{-1.07-0.43} \times 10^{-3}$	1.28–1.40	1.34	399	1.7	$2.28^{+0.15+0.17}_{-0.15-0.17} \times 10^{-2}$
0.37–0.41	0.39	44	0.0	$8.05^{+1.63+0.39}_{-1.49-0.39} \times 10^{-3}$	1.40–1.53	1.47	412	3.5	$2.07^{+0.14+0.16}_{-0.14-0.16} \times 10^{-2}$
0.41–0.44	0.42	56	0.0	$9.19^{+1.65+0.45}_{-1.42-0.45} \times 10^{-3}$	1.53–1.68	1.60	466	6.2	$2.10^{+0.14+0.17}_{-0.14-0.17} \times 10^{-2}$
0.44–0.48	0.46	68	0.0	$9.95^{+1.58+0.51}_{-1.46-0.51} \times 10^{-3}$	1.68–1.84	1.75	485	9.0	$1.91^{+0.13+0.16}_{-0.13-0.16} \times 10^{-2}$
0.48–0.53	0.50	87	0.0	$1.14^{+0.16+0.06}_{-0.15-0.08} \times 10^{-2}$	1.84–2.01	1.92	555	11.5	$2.05^{+0.13+0.17}_{-0.12-0.17} \times 10^{-2}$
0.53–0.57	0.55	84	0.0	$9.30^{+1.41+0.52}_{-1.32-0.52} \times 10^{-3}$	2.01–2.20	2.11	632	12.9	$2.18^{+0.12+0.17}_{-0.12-0.17} \times 10^{-2}$
0.57–0.63	0.60	122	0.0	$1.26^{+0.15+0.07}_{-0.14-0.07} \times 10^{-2}$	2.20–2.41	2.31	622	13.7	$1.88^{+0.11+0.16}_{-0.11-0.16} \times 10^{-2}$
0.63–0.68	0.65	131	0.0	$1.20^{+0.14+0.07}_{-0.13-0.07} \times 10^{-2}$	2.41–2.64	2.53	678	13.8	$1.95^{+0.11+0.16}_{-0.11-0.16} \times 10^{-2}$
0.68–0.75	0.71	154	0.0	$1.32^{+0.14+0.08}_{-0.14-0.08} \times 10^{-2}$	2.64–2.89	2.76	637	13.3	$1.77^{+0.10+0.15}_{-0.10-0.15} \times 10^{-2}$
0.75–0.82	0.78	157	0.0	$1.30^{+0.15+0.08}_{-0.14-0.08} \times 10^{-2}$	2.89–3.16	3.00	494	12.5	$1.90^{+0.12+0.22}_{-0.12-0.23} \times 10^{-2}$
0.82–0.89	0.86	209	0.0	$1.84^{+0.17+0.11}_{-0.16-0.11} \times 10^{-2}$	3.16–3.46	3.28	213	11.5	$1.64^{+0.18+0.22}_{-0.17-0.22} \times 10^{-2}$
0.89–0.98	0.94	194	0.0	$1.51^{+0.15+0.10}_{-0.14-0.10} \times 10^{-2}$					

calculated near 2 GeV to reduce modulation effects. Both are consistent with solar-minimum secondary calculations. Neither exhibits the flattening at low energies found by BESS95 + 97, although the differences are statistically small.

The evident differences among the calculations shown in Fig. 2 arise from several factors that can affect the normalization or shape of the spectrum: (1) definition of the primary proton and helium spectra, (2) incomplete knowledge of nuclear physics in propagation, (3) parameters and

FIG. 2.   Solar-minimum BESS-Polar II, BESS95 + 97, and PAMELA TOA $\bar{p}$ fluxes and secondary model calculations.

models of propagation in the Galaxy, and (4) modulation in the heliosphere. Variation in the absolute fluxes of interstellar protons and helium, for instance, affects the absolute flux of $\bar{p}$'s but not the spectral shape.

Precise measurement of the low-energy $\bar{p}$ spectrum by BESS-Polar II allows secondary flux calculations to be evaluated by comparing observed and predicted spectral shapes, as shown in Fig. 3. The calculations are normalized to BESS-Polar II at 2 GeV to focus on their shapes. The calculated spectra and data points are also multiplied by E_k^{-1} to emphasize differences at low energies. The observed data are not normalized. χ^2, calculated with BESS-Polar II data and the normalized secondary $\bar{p}$ calculations in Fig. 3, are 0.61 (1), 0.61 (2), 1.32 (3), 1.70 (4), and 0.67 (5). The shape variation from uncertainty in the level of solar modulation is illustrated by the lower shaded band, calculated with the Mitsui et al. model [6,22] and modulation parameters of 500 MV ($\chi^2 = 0.81$) and 700 MV ($\chi^2 = 0.52$). The small sensitivity of drift calculations to tilt angle is shown by the upper shaded band using $A < 0$ Bieber et al. data [23] at 10° and 20° (interpolated). In both cases, the change in spectral shape is small compared to differences arising from propagation models because of the peaked shape of the LIS secondary $\bar{p}$ spectrum. BESS-Polar II results are more consistent with models (curves 1, 2, and 5) without low-energy $\bar{p}$'s from tertiary interactions (curve 3) or a soft spectrum from diffusive reacceleration (curve 4).

The likelihood of primary $\bar{p}$'s from PBH evaporation can be quantified by a model-dependent evaporation rate ($\mathcal{R}$) determined by fitting a PBH model spectrum to the difference of a secondary calculation from the measured flux. $\mathcal{R}$ is positive (physical) only if the measured flux exceeds the
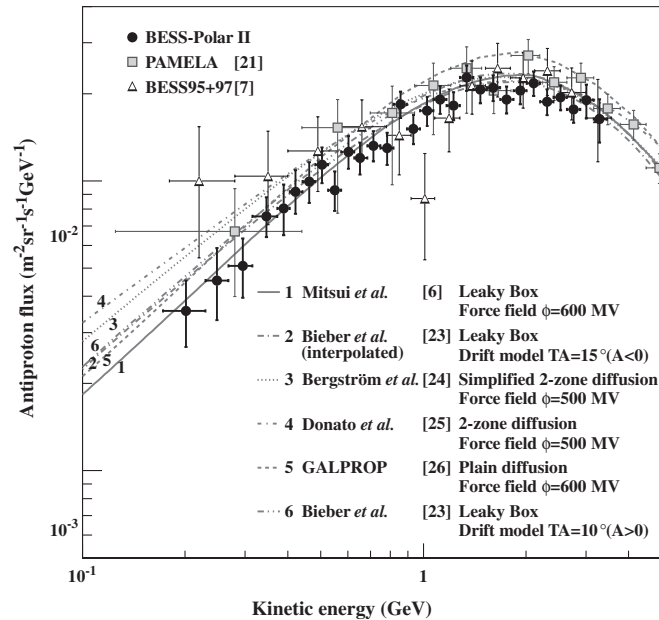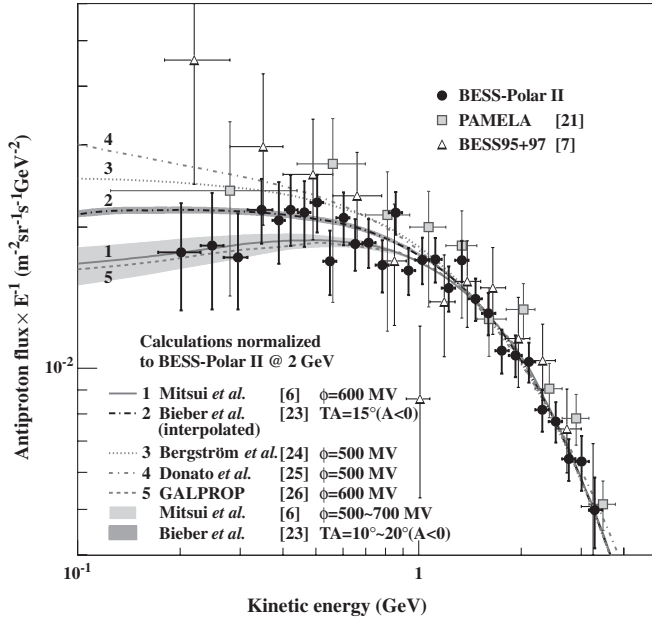
FIG. 3. Comparison of $\bar{p}$ flux shapes with secondary calculations normalized to BESS-Polar II flux at 2 GeV. Sensitivity to uncertainty in the force-field modulation parameter is shown by the lower shaded band. The small sensitivity of secondary $\bar{p}$ drift calculations at solar minimum to tilt angle is illustrated by the upper shaded band.

FIG. 4. (Top) Possible primary $\bar{p}$ fluxes from PBH evaporation calculated for (A) BESS-Polar II and (B) BESS95 + 97 by fitting differences of the measured spectra from the Mitsui secondary $\bar{p}$ spectrum. (Bottom) PBH evaporation rate ($\mathcal{R}$) distributions. Values of $\mathcal{R} < 0$ are nonphysical.

secondary prediction. To avoid bias from uncertainties in the predicted absolute flux, the secondary calculation is normalized to the measurements at the spectral peak (2 GeV), as in Fig. 3. Comparing the models shown in Fig. 3 to the measurements, only 1 and 5 give a significant, and almost identical, excess. We use curve 1, a slightly better fit to the measured spectrum, to calculate $\mathcal{R}$. Using the Maki *et al.* PBH model [5] with force-field modulation gives $\mathcal{R} = 5.0^{+4.1}_{-4.0} \times 10^{-4}$ pc^{-3} yr^{-1}, as shown in Fig. 4. This excludes by more than 9 sigma the slight possibility of primary $\bar{p}$'s suggested by $\mathcal{R} = 4.2^{+1.8}_{-1.9} \times 10^{-3}$ pc^{-3} yr^{-1} from BESS95 + 97 data with the same models and modulation. We also find a 90% confidence level upper limit of $\mathcal{R} \sim 1.2 \times 10^{-3}$ pc^{-3} yr^{-1}. This is almost insensitive to modulation (500 MV: $\mathcal{R} = 1.0 \times 10^{-3}$ pc^{-3} yr^{-1}; 600 MV: $\mathcal{R} = 1.2 \times 10^{-3}$ pc^{-3} yr^{-1}; 700 MV: $\mathcal{R} = 1.3 \times 10^{-3}$ pc^{-3} yr^{-1}).

The effects of charge-sign-dependent modulation in the $A > 0$ and $A < 0$ solar magnetic field polarities on secondary and possible PBH primary $\bar{p}$ fluxes differ considerably because of their spectral shapes. Curves 2 and 6 in Fig. 2 indicate that the differences in the solar-minimum secondary fluxes are small. However, the predicted LIS PBH $\bar{p}$ spectrum peaks near the lower end of the BESS-Polar II energy range, and solar polarity would strongly affect the contribution of primaries to the measured low-energy flux. The primary $\bar{p}$ flux should be suppressed for $A > 0$ and higher for $A < 0$. Thus, solar polarity cannot explain the
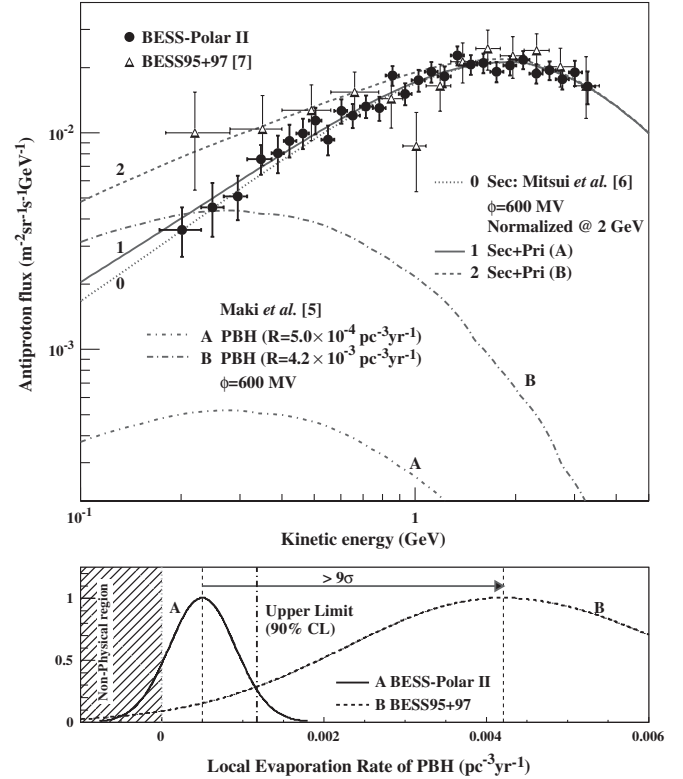
excess reported by BESS95 + 97 or the negligible excess in the BESS-Polar II results reported here. Within statistics, the BESS-Polar II data show no evidence of primary $\bar{p}$'s from PBH evaporation.

*Corresponding author.
Present address: NASA-Goddard Space Flight Center (NASA-GSFC), Greenbelt, MD 20771, USA.
Kenichi.Sakai@nasa.gov

[1] T. K. Gaisser and R. K. Schaefer, Astrophys. J. **394**, 174 (1992).
[2] K. Yoshimura, Adv. Space Res. **27**, 693 (2001).
[3] A. W. Strong, I. V. Moskalenko, and O. Reimer, Astrophys. J. **613**, 962 (2004).
[4] S. W. Hawking, Commun. Math. Phys. **43**, 199 (1975).

[5] K. Maki, T. Mitsui, and S. Orito, Phys. Rev. Lett. **76**, 3474 (1996).

[6] T. Mitsui, K. Maki, and S. Orito, Phys. Lett. B **389**, 169 (1996).

[7] S. Orito *et al.*, Phys. Rev. Lett. **84**, 1078 (2000).

[8] J. W. Mitchell *et al.*, Nucl. Phys. B, Proc. Suppl. **134**, 31 (2004).

[9] A. Yamamoto *et al.*, Adv. Space Res. **30**, 1253 (2002).

[10] T. Yoshida *et al.*, Adv. Space Res. **33**, 1755 (2004).

[11] Y. Ajima *et al.*, Nucl. Instrum. Methods Phys. Res., Sect. A **443**, 71 (2000).

[12] S. Haino *et al.*, Nucl. Instrum. Methods Phys. Res., Sect. A **518**, 167 (2004).

[13] S. Haino *et al.*, Phys. Lett. B **594**, 35 (2004).

[14] A. Yamamoto *et al.*, Adv. Space Res. **42**, 442 (2008).

[15] K. Yoshimura *et al.*, Adv. Space Res. **42**, 1664 (2008).

[16] M. Sasaki *et al.*, Adv. Space Res. **42**, 450 (2008).

[17] K. Abe *et al.*, Phys. Lett. B **670**, 103 (2008).

[18] Y. Asaoka *et al.*, Nucl. Instrum. Methods Phys. Res., Sect. A **416**, 236 (1998).

[19] S. A. Stephens, Astropart. Phys. **6**, 229 (1997).

[20] K. Yamato *et al.*, Phys. Lett. B **632**, 475 (2006).

[21] O. Adriani *et al.*, Phys. Rev. Lett. **105**, 121101 (2010).

[22] T. Mitsui, Ph.D. thesis, University of Tokyo, 1996.

[23] J. W. Bieber *et al.*, Phys. Rev. Lett. **83**, 674 (1999); J. W. Bieber (private communication).

[24] L. Bergström, J. Edsjo, and P. Ullio, Astrophys. J. **526**, 215 (1999).

[25] F. Donato *et al.*, Astrophys. J. **563**, 172 (2001).

[26] A. W. Strong and I. V. Moskalenko, Astrophys. J. **509**, 212 (1998).